Direct fluorescent-dye labeling of α-tubulin in mammalian cells for live cell and superresolution imaging

Tomer Schvartz[a,b], Noa Aloush[b,c], Inna Goliand[a,b], Inbar Segal[a,b], Dikla Nachmias[a,b], Eyal Arbely[b,c], and Natalie Elia[a,b,*]

[a]Department of Life Sciences and [c]Department of Chemistry, Ben-Gurion University of the Negev, Beer Sheva 84105, Israel; [b]The National Institute for Biotechnology in the Negev, Beer Sheva 84105, Israel

ABSTRACT **Genetic code expansion and bioorthogonal labeling provide for the first time a way for direct, site-specific labeling of proteins with fluorescent-dyes in live cells. Although the small size and superb photophysical parameters of fluorescent-dyes offer unique advantages for high-resolution microscopy, this approach has yet to be embraced as a tool in live cell imaging. Here we evaluated the feasibility of this approach by applying it for α-tubulin labeling. After a series of calibrations, we site-specifically labeled α-tubulin with silicon rhodamine (SiR) in live mammalian cells in an efficient and robust manner. SiR-labeled tubulin successfully incorporated into endogenous microtubules at high density, enabling video recording of microtubule dynamics in interphase and mitotic cells. Applying this labeling approach to structured illumination microscopy resulted in an increase in resolution, highlighting the advantages in using a smaller, brighter tag. Therefore, using our optimized assay, genetic code expansion provides an attractive tool for labeling proteins with a minimal, bright tag in quantitative high-resolution imaging.**

Monitoring Editor
Jennifer Lippincott-Schwartz
Howard Hughes Medical Institute

Received: Mar 13, 2017
Revised: Aug 14, 2017
Accepted: Aug 16, 2017

INTRODUCTION

Over the past two decades, fluorescent proteins (Fl-proteins) such as green fluorescent protein (GFP) have been routinely used for fluorescence tagging of proteins in live cell applications. The use of Fl-proteins has, however, several drawbacks that stem from their relatively large size (GFP, 27 kDa, ~5 nm) and moderate photophysical properties (van de Linde *et al.*, 2012). As a result, the spatiotemporal resolution of current high-end microscopy techniques, including superresolution (SR) microscopy, cannot be exploited to their full potential (Henriques *et al.*, 2011; van de Linde *et al.*, 2012). On top of that, the use of a large protein tag is prone to produce measurement artifacts as it may affect the dynamics and ultrastructural organization of the protein studied. This problem is more pronounced in the study of macromolecular complexes and cellular polymers, which rely on numerous, intimate protein–protein interactions to mediate their function. To overcome the limitations associated with Fl-proteins, several approaches for tagging proteins with organic fluorescent dyes (Fl-dyes) have been applied in recent years to live cell and SR imaging (e.g., SNAP-tag, CLIP-tag, HaloTag; reviewed in Reymond *et al.*, 2011; van de Linde *et al.*, 2012; Lang and Chin, 2014). These technologies overcome the photophysical constrains of Fl-proteins; however, they still suffer from the limitation of relying on the conjugation of a relatively large protein tag.

Recently an elegant alternative to Fl-protein tagging has been proposed and demonstrated (Lang *et al.*, 2012b; Nikic and Lemke, 2015; Uttamapinant *et al.*, 2015; Peng and Hang, 2016). In this approach, proteins are site-specifically labeled through direct binding of a Fl-dye to a noncanonical amino acid (NCAA), integrated in the amino acid sequence of the tagged protein. Incorporation of the NCAA into the amino acid sequence of the protein is carried out

This article was published online ahead of print in MBoC in Press (http://www.molbiolcell.org/cgi/doi/10.1091/mbc.E17-03-0161) on August 23, 2017.

Author contributions: T.S. performed all experiments and was involved in designing the experiments and in interpreting the results. N.A. performed experiments in assay optimization and was responsible for plasmid optimization and cloning. I.G. performed live cell imaging of mitotic cells and helped with SIM imaging. I.S. performed viability assays. D.N. provided technical help, performed experiments, and was involved in interpreting the results. E.A. was involved in experimental design, in data analysis, and in writing the manuscript. N.E. designed the experiments, performed EB1 particle tracking and SIM measurements, was in charge of data analysis, and wrote the manuscript.

*Address correspondence to: Natalie Elia (elianat@post.bgu.ac.il).

Abbreviations used: AA, amino acid; BCNK, bicyclo[6.1.0]nonyne-lysine; BCN-Lys, bicyclo[6.1.0]nonyne-lysine; Boc-Lys, Nε-tertbutyloxycarbonyl lysine; 3D, three-dimensional; DOC, deoxycholate; FBS, fetal bovine serum; Fl-dyes, fluorescent dyes; Fl-proteins, fluorescent proteins; FSM, fluorescent speckle microscopy; FWHM, full-width at half-maximum; GCE, genetic code expansion; GFP, green fluorescent protein; MT, microtubule; NCAA, noncanonical amino acid; NES, nuclear export signal; PBS, phosphate-buffered saline; PFA, paraformaldehyde; SFL-TAG, site-specific, Fl-dye, live labeling TAG-based approach; SIM, structured illumination microscopy; SiR-Tet, tetrazine-conjugated silicon-rhodamine; SNR, signal-to-noise ratio; SR, superresolution microscopy.

through methods of genetic code expansion (GCE) (reviewed in Johnson *et al.*, 2010; Davis and Chin, 2012). Genetic code expansion utilizes an orthogonal tRNA/tRNA-synthetase pair to direct the incorporation of a NCAA in response to a unique codon, usually the amber stop codon (TAG), which is inserted in-frame to the nucleotide sequence of a protein. Together with ultrafast and specific bioorthogonal reactions, such as the fluorogenic inverse electron-demand Diels-Alder reaction between a NCAA carrying a strained alkyne and a tetrazine-conjugated Fl-dye, this approach provides an essentially direct way for labeling proteins in live cells with Fl-dyes (see Figure 1A for an illustration of the approach; Blackman *et al.*, 2008; Lang *et al.*, 2012a; Plass *et al.*, 2012; Lang and Chin, 2014). Here we refer to this Site-specific, Fl-dye, Live-labeling, TAG-based approach as: SFL-TAG.

Although this approach was introduced several years ago and genetic code expansion has, since then, been demonstrated in mammalian cultured cells as well as in whole organisms (Greiss and Chin, 2011; Bianco *et al.*, 2012; Elsasser *et al.*, 2016; Ernst *et al.*, 2016), it has yet to be exploited in cell biology applications. In this work, we have explored the feasibility of SFL-TAG for live cell and SR imaging by optimizing reaction conditions for α-tubulin labeling. After a series of calibration and optimization steps, we successfully incorporated the NCAA bicyclo[6.1.0]nonyne-lysine (BCN-Lys) into α-tubulin and performed direct Fl-dye labeling of α-tubulin in live cells with tetrazine-conjugated silicon-rhodamine (SiR-Tet) at positions G45 and A278. BCN-Lys α-tubulin labeled with SiR-Tet (SiR-BCNK-tubulin) incorporated into the microtubule (MT) network of interphase and mitotic cells, validating the approach. Careful optimization of the labeling reaction significantly improved the signal-to-noise ratio (SNR) and dramatically increased the proportion of labeled cells in the population. With these optimized conditions, we were able to 1) record MT dynamics in live interphase and mitotic cells, 2) perform two-color imaging (in combination with Fl-proteins), and 3) visualize MTs at subdiffraction resolution using structured illumination microscopy (SIM). We therefore conclude that under our optimized conditions, SFL-TAG is an applicable approach for labeling macromolecular complexes in mammalian cells for live cell and SIM imaging applications.

RESULTS AND DISCUSSION

One of the advantages of SFL-TAG is its flexibility in choosing the labeling site. The NCAA can essentially be inserted at any given location along the protein sequence. However, the level of amino acid incorporation (i.e., amber suppression efficiency) is context-dependent and may vary significantly between different positions (Pott *et al.*, 2014). Therefore, we began by screening for different potential NCAA incorporation sites in α-tubulin. For the initial screen, we chose five different sites, G34, G45, K163, A278, and A427. These sites were selected because they represent different localities along the linear sequence of the polypeptide (start to end). Importantly, according to α-tubulin sequence annotation (UniProt) and Protein Data Bank (PDB) structures these sites are not predicted to be involved in either protein–protein interactions or posttranslational modifications and were not reported in the literature as essential for tubulin structure or function (Figure 1B).

To genetically encode the incorporation of a NCAA into a selected protein, several components need to be introduced to cells. These components include: an orthogonal $tRNA_{CUA}$, a tRNA synthetase capable of aminoacylating its cognate tRNA with a

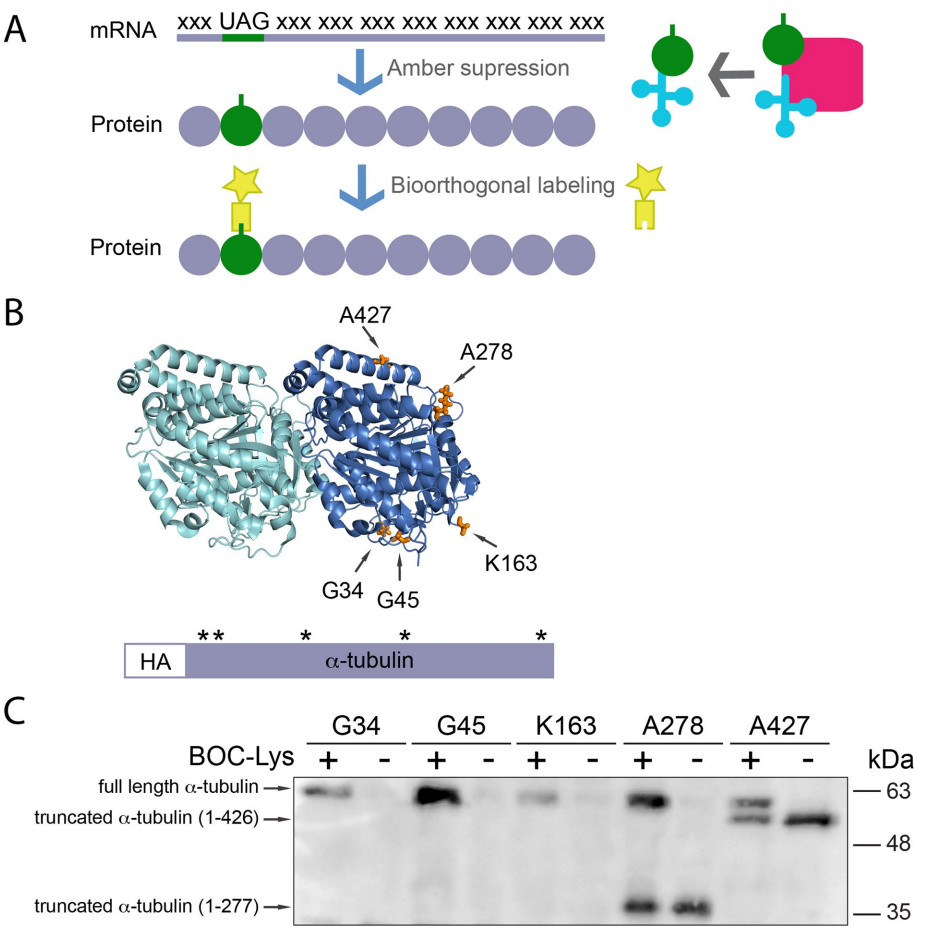

FIGURE 1: Incorporating a NCAA into α-tubulin in mammalian cells. (A) Schematic view of the experimental approach. An in-frame TAG stop codon is inserted to the nucleotide sequence of the protein. During translation, the TAG is recognized by an orthogonal $tRNA_{CUA}$ (blue) that was charged with the NCAA (green) by its cognate orthogonal synthetase (magenta). Next the NCAA carrying a strained alkyne (green) reacts with a tetrazine-conjugated Fl-dye (yellow) that is introduced to the cells, giving rise to direct labeling of the protein with Fl-dye. Plasmid maps and chemical structures of the NCAAs and tetrazine bound Fl-dye used in this study are presented in Supplemental Figure S1. (B) PDB structure of an α (dark blue) and β (cyan) tubulin dimer (PDB ID: 5IJ0). Positions selected for NCAA incorporation (orange) in α-tubulin are marked with arrows. A scheme of the inserted α-tubulin gene is shown below. Asterisks indicate the relative locations of the selected positions along the gene. (C) HEK293T cells were transfected with pBUD-Pyl-RS-tub that carries α-tubulin with a TAG codon at the indicated positions and were incubated for 24 h in the presence or absence of the NCAA Boc-Lys. Cells were then harvested and subjected to Western blot analysis using anti-HA antibodies. Results indicate that full-length α-tubulin is expressed only upon addition of the NCAA. Lower molecular weight bands in A278 and A427 mutations represent truncated versions of α-tubulin due to translation of α-tubulin that terminates at the in-frame TAG stop codon mutation.

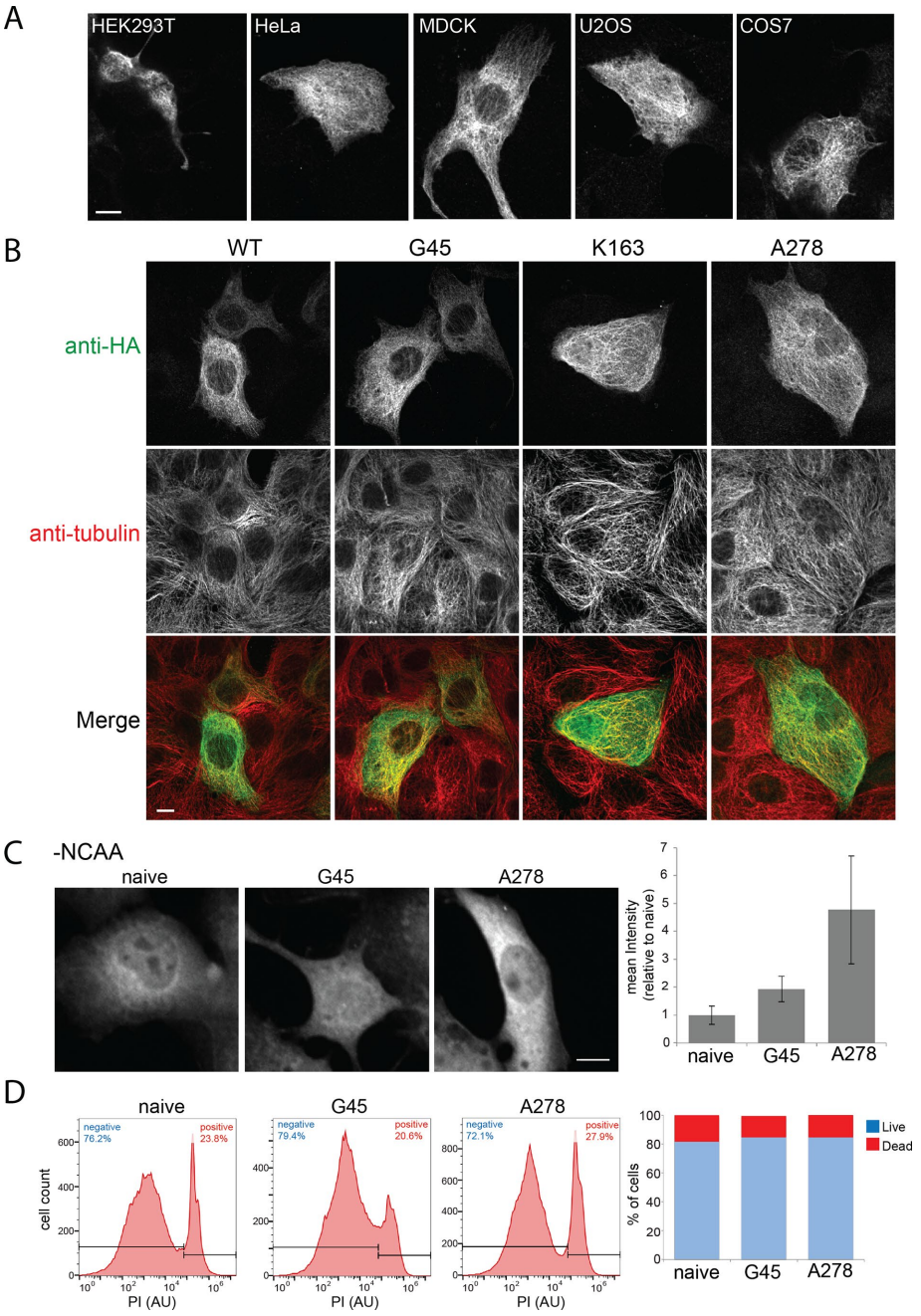

FIGURE 2: NCAA modified α-tubulin incorporates into the cellular MT network. (A) Cells were transfected with pBUD-Pyl-RS-tub that carries tubulin^{45TAG}, incubated for 24 h in the presence of Boc-Lys, and stained with anti-HA antibodies. Shown are single Z slices from representative cells. $n = 10$; scale bar, 10 μm. (B) MDCK cells were transfected with pBUD-Pyl-RS-tub that carries α-tubulin with a TAG codon at the designated positions and incubated for 24 h in the presence of Boc-Lys. Cells were then stained with anti-HA and anti–α-tubulin antibodies. Shown are single Z slices from representative cells. $n = 10$; scale bar, 10 μm. (C) Naïve COS7 cells or COS7 cells transfected with pBUD-BCNK-RS-tub that carries tubulin^{45TAG} or tubulin^{278TAG} were incubated for 48 h in the absence of NCAA, fixed, and stained with anti-HA antibodies. Shown are maximum intensity projections. Graph on right shows the relative mean intensity of HA staining measured in cells at the indicated conditions. Intensity levels were normalized to naïve cells. $n = 45$; scale bar, 10 μm. (D) COS7 cells were transfected with pBUD-BCNK-RS-tub that carries tubulin^{45TAG} or tubulin^{278TAG} and incubated for 48 h in the absence of NCAA and subjected to PI flow cytometry analysis. Shown are PI plots from a representative experiment. An average of the percent of live and dead cells in each treatment as obtained in three independent experiments is presented in the graph to the right.

chosen NCAA, a modified gene that carries an in-frame amber stop codon, and the NCAA. We have previously shown that the level of NCAA incorporation in cultured mammalian cells is increased upon compiling all the genetic components into a single expression vector (Cohen and Arbely, 2016). Modified α-tubulin cDNA sequences carrying a TAG codon at the selected sites were therefore inserted into the single vector system (pBUD-Pyl-RS-tub vector; Supplemental Figure S1B). An HA tag was added at the N terminal of all α-tubulin versions to allow for antibody detection of the modified tubulin. To evaluate the level of NCAA incorporation in response to an in-frame stop codon, expression levels of full-length α-tubulin were examined in HEK293T cells transfected with different pBUD-Pyl-RS-tub variants, carrying a TAG codon at selected positions in α-tubulin, in the presence or absence of the cell permeable NCAA. For this initial evaluation step, we examined the incorporation of the widely used NCAA Nε-tert-butyloxycarbonyl lysine (Boc-Lys) (Yanagisawa *et al.*, 2008). Western blot analysis showed that NCAA incorporation was attained in all the five sites chosen for the initial screen, with maximum expression levels of full-length α-tubulin obtained using positions G45 and A278 (Figure 1C). On the basis of these results, we have decided to continue our optimization process for α-tubulin tagging with positions G45 and A278. Position K163 was also selected for future optimization, regardless of amber suppression efficiency, since recombinant yeast α-tubulin, site-specifically modified with azido-lysine in this site, was previously shown to polymerize into MTs in vitro (Kleiner *et al.*, 2013). Notably, the successful incorporation of Boc-Lys into all selected positions in α-tubulin highlights the robustness of GCE and indicates that SFL-TAG indeed provides flexibility in choosing the site of incorporation. In practical terms, these results demonstrate that finding a suitable NCAA incorporation site is not a limiting factor of SFL-TAG.

We next asked whether α-tubulin proteins that carry the NCAA are able to incorporate into MTs in different cell lines. For that, we transfected cells with pBUD-Pyl-RS-tub^{45TAG} in the presence of Boc-Lys and immunostained them 24 h later with anti-HA antibodies. The results clearly indicate that the modified α-tubulin is capable of incorporating into MTs in all the cell lines tested: HEK293T, HeLa, Madin-Darby canine kidney (MDCK), U2OS and COS7 (Figure 2A).

Comparable results were obtained for two additional amber suppression sites, K163 and A278, in MDCK cells (Figure 2B). We therefore concluded that positions G45, K163, and A278 are suitable sites for incorporating a NCAA into α-tubulin in cell biology applications.

One possible concern associated with GCE is the formation of a truncated version of the protein, which results from introducing a premature stop codon to the nucleotide sequence of the protein. Indeed, truncated versions of α-tubulin were seen upon inserting a TAG codon in positions A278 and A427 (Figure 1C). Truncated α-tubulin was not detected in Western blot analysis upon mutating positions G34, G45, or K163. To further evaluate the cellular levels of truncated α-tubulin, we have transfected cells with plasmids carrying a TAG codon in positions G45 and A278 in α-tubulin in the absence of NCAA and immunostained them with anti-HA antibodies. At these conditions the in-frame TAG should function only as a stop codon and not as a coding codon. A twofold increase in HA-staining fluorescence intensity levels was measured in cells expressing tub^{45TAG} compared with naïve (nontransfected) cells (Figure 2C). A much higher increase in intensity (approximately fivefold) was measured in cells expressing tub^{278TAG}. This means that, consistent with Western blot results, there is considerably less truncated α-tubulin in cells upon mutating position G45 for NCAA incorporation than upon mutating position A278. This may result from degradation of the short length α-tubulin polypeptide that is synthesized under these conditions (44 amino acids [AA]). High levels of truncated α-tubulin can potentially be toxic to cells. However, based on a flow cytometry assay, even under these maximal truncation formation levels (without a NCAA) no effect on cell viability was observed in response to mutating either position (Figure 2D). It should be noted that this result does not rule out milder cellular effects induced by the truncations. At this point we therefore decided to continue our calibration using all three positions verified above (G45, K163, A278). But, to minimize possible effects of truncated α-tubulin we find position G45 more suitable for live cell imaging of tubulin.

Having competent positions for NCAA incorporation, we turned to calibrating the bioorthogonal reaction required for the labeling step. In this work, we used the well-established bioorthogonal reaction between BCN-Lys and tetrazine-Fl-dye (Lang *et al.*, 2012b). For incorporating BCN-Lys into the selected sites in α-tubulin, we used a pBUD-BCNK-RS-tub vector that carries an evolved BCN-Lys specific synthetase (Supplemental Figure S1B). As expected, BCN-Lys incorporated into all the selected positions in α-tubulin, leading to expression of the full-length protein (Supplemental Figure S2A). The tetrazine moiety can, in principle, be conjugated to any Fl-dye, providing great flexibility in terms of wavelength and dye properties. Among the cell permeable dyes, SiR was previously shown to be superior with respect to background staining, a key property of Fl-dyes in live cell applications (Lukinavicius *et al.*, 2013). We therefore used SiR conjugated to tetrazine (SiR-Tet; Supplemental Figure S1A) in our study. Indeed, very little background fluorescence was observed for SiR-Tet at calibrated washing conditions (Supplemental Figure S2B). The minimal stickiness properties of SiR-Tet, together with the fluorogenic nature of the BCN-tetrazine reaction (Lang *et al.*, 2012b), provide a good starting point for live cell labeling.

Labeling experiments began by evaluating the accessibility of the three chosen BCN-Lys incorporation sites (G45, K163, A278) to SiR-Tet labeling (Figure 3A). Addition of SiR-Tet to cells expressing α-tubulin carrying BCN-Lys at position G45 or A278 showed clear MT labeling. SiR fluorescence was also clearly detected in MTs of the mitotic spindle (Supplemental Figure S2C), confirming that both stable and dynamic MT structures are labeled. However, no MT labeling was observed when position K163 was used for BCN-Lys incorporation (Figure 3A). This result may suggest that position 163 is inaccessible for tetrazine binding or that the addition of SiR at position 163 inhibits the incorporation of labeled α-tubulin into MTs. Therefore, when calibrating labeling conditions, both the effect of NCAA incorporation and of Fl-dye binding should be considered. To evaluate specificity of labeling, a competition assay using a tetrazine version that is not conjugated to a Fl-dye (tetrazine-NH_2; Supplemental Figure S1A) was performed. As expected, MT labeling was completely abolished at high concentrations of tetrazine-NH_2 (Supplemental Figure S2D). Taking the results together, we conclude that positions G45 and A278 are suitable sites for bioorthogonal labeling of α-tubulin.

Although we have successfully demonstrated direct labeling of α-tubulin using SFL-TAG, our assay still suffered from several limitations. Mainly, the percentage of cells exhibiting MT labeling was poor (5%) and the SNR measured (1.5) was too low to allow high-end imaging (Table 1, top row, and Supplemental Figure S3). Additionally, we experienced difficulties in cotransfecting cells with GFP-tagged proteins for performing two-color imaging. By conducting a series of calibrations for key steps in the SFL-TAG protocol (Table 1), we were able to considerably increase the percentage of cells with labeled MTs (up to 33%) and to improve SNR (up to 1.75; Supplemental Figure S3). Noticeably, we found that addition of the oxygen scavenger ascorbic acid to the growth media greatly increased the percentage of MT labeled cells (from 10% to 25%; Table 1 and Supplemental Figure S3E). Using the calibrated conditions, cotransfection could also be readily achieved (Figure 3, B, D, and E). Flow cytometry analysis of cell viability revealed that the population of HEK293T or COS7 cells labeled using the calibrated protocol does not exhibit an increase in the percentage of dead cells (Supplemental Figure S4). We therefore find these conditions suitable for routine high-end imaging of MTs in live cells (the optimized protocol is provided in the Supplemental Information).

To ensure that MTs labeled through SFL-TAG of α-tubulin represent the cellular MT pool, we measured the extent of colocalization between GFP-tubulin and SiR-BCNK-tubulin. A similar pattern of MT labeling was observed in both channels (Figure 3B, top panel). One obvious difference between the channels was the nuclear labeling observed in the SiR channel. Unspecific nuclear labeling has been previously reported for SFL-TAG and ongoing research in the field is advancing toward overcoming this issue (Uttamapinant *et al.*, 2015; Nikic *et al.*, 2016). However, since MTs do not localize to the nucleus, this unspecific labeling did not interfere with our imaging and was therefore not addressed in this study. Quantitative comparison of the overall colocalization level between the channels resulted in a GFP/SiR Pearson correlation ratio of 0.54 (Figure 3B, top panel). This relatively low value probably stems from the unspecific SiR staining observed at the nucleus. Indeed, calculating the Pearson correlation for regions outside the nucleus resulted in an average value of 0.95 (GFP/SiR; Figure 3B, middle panel), indicating an essentially identical coverage of cellular MTs with GFP-tubulin and SiR-BCNK-tubulin. Line-scan intensity profiles measured across individual fibers produced similar patterns for GFP and SiR, showing that individual MT filaments are similarly labeled by both fluorophores (Figure 3B, bottom panel). Therefore, it appears that both SiR-BCNK-tubulin and GFP-tubulin incorporate with similar proportions to MT fibers, demonstrating that SFL-TAG is, at the minimum, comparable with GFP labeling on MTs.

Next we asked whether MT posttranslational modifications and dynamics are affected in cells with SiR-BCNK-tubulin labeled MTs. Overall the MT K40 acetylation pattern appeared similar in naïve

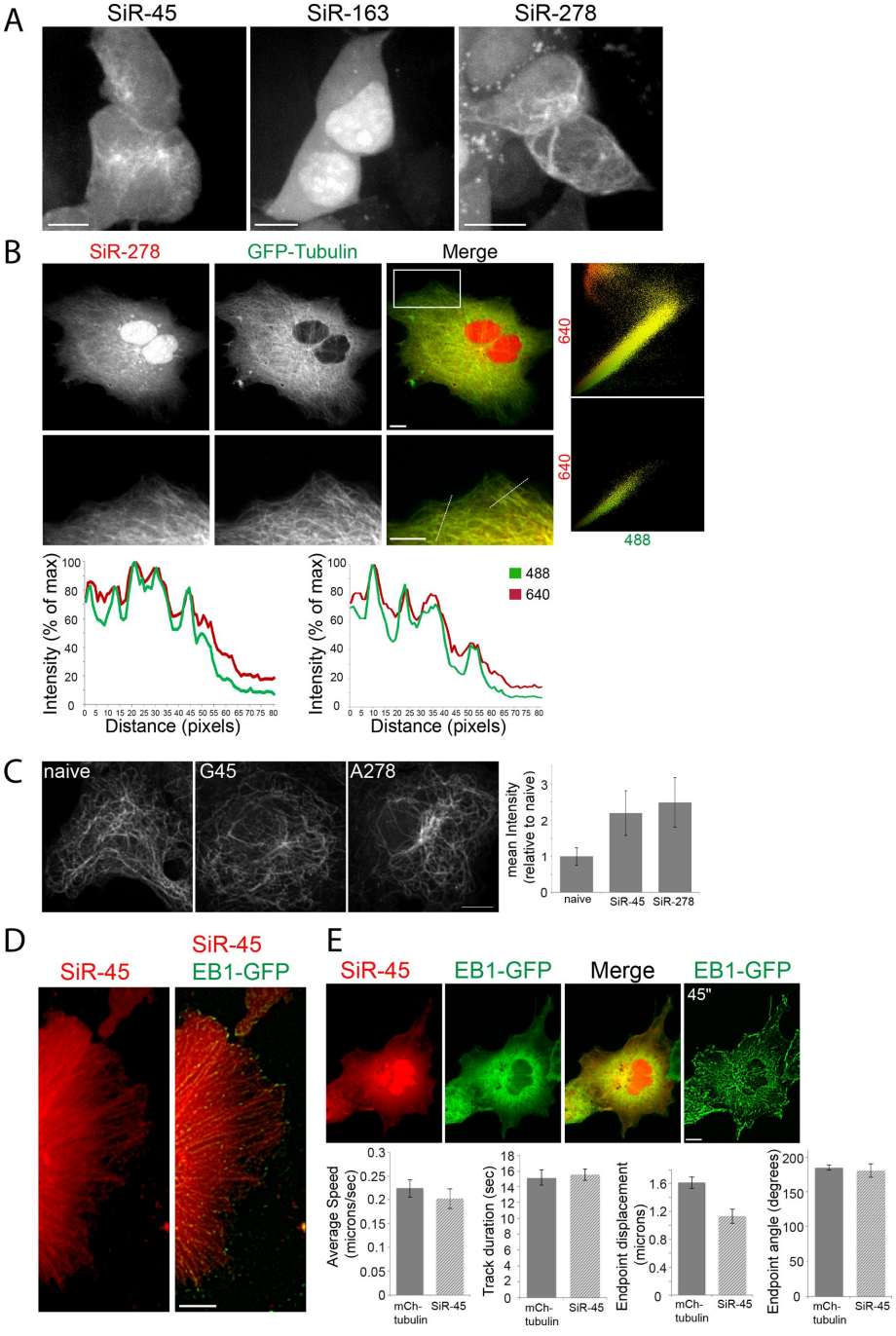

FIGURE 3: SiR labeling of NCAA modified α-tubulin in live cells does not interfere with MT organization and dynamics. (A) HEK293T cells were transfected with pBUD-BCNK-RS-tub that carries α-tubulin with a TAG codon at the indicated positions, incubated for 24 h in the presence of BCN-Lys, and labeled with SiR-Tet (1 h) for α-tubulin labeling. Shown are maximum intensity projections of representative cells. Note that while microtubule labeling was clearly observed with α-tubulin labeled on positions 45 and 278, no labeling was observed when position 163 was labeled. $n = 10$; scale bar, 10 μm. (B) SiR-BCNK-tubulin colocalizes with GFP-tubulin on microtubules. COS7 cells were cotransfected with pBUD-BCNK-RS-tub^{278TAG} and with GFP-tubulin, incubated for 48 h in the presence of BCN-Lys, and labeled (1 h) with SiR-Tet. Shown are maximum intensity projections of a representative cell. Zoomed-in images of a subset of the cell (corresponds to rectangle in upper panel) are shown in the middle panel. Overall colocalization analysis between 488 (GFP) and 640 (SiR) channels is shown in right panel (entire cell, top; subset of the cell, bottom). Line intensity profiles of both 488 and 640 channels, corresponding to the dashed lines plotted in the subset image, are plotted in bottom panel. Note that a very similar pattern is observed in both channels, indicating a high degree of colocalization between the channels. $n = 5$; scale bar, 10 μm. (C) COS7 cells were transfected with pBUD-BCNK-RS-tub^{45TAG} or pBUD-BCNK-RS-tub^{278TAG}, incubated for 48 h in the presence of BCN-Lys, and labeled (1 h) with SiR-Tet. Cells were then fixed and stained with acetylated tubulin antibodies. Shown are maximum intensity projections of acetylated tubulin staining from representative cells. The relative mean intensity of acetylated tubulin staining measured in cells at the indicated conditions is displayed in the graph on the right. Intensity levels were normalized to naïve cells. $n = 20$; scale bar, 10 μm. (D, E) EB1 localization and dynamics on microtubules are not perturbed in the presence of SiR-BCNK-tubulin. COS7 cells were cotransfected with pBUD-BCNK-RS-tub^{45TAG} and with EB1-GFP and incubated for 48 h in the presence of BCN-Lys and labeled with SiR-Tet. Clear EB1 decoration at the plus end of microtubules labeled with SiR-BCNK-tubulin is observed. (D) Microtubule growth was calculated from 45-s-long video recordings acquired at 2 s intervals for EB1, in cells exhibiting SiR-BCNK-tubulin labeled microtubules. (E) A representative cell is shown in the top panel. A time composite image of EB1 time series is shown in the top right panel. Average speed, track duration, endpoint displacement, and endpoint angle were calculated using particle tracking as described in *Materials and Methods*. For comparison, similar experiments and analysis were performed in COS7 cells cotransfected with EB1-GFP and mCherry-tubulin. Results are summarized in the bottom panel. Shown are maximum projection images. $n = 14$ (D), $n = 5$ (E), scale bar, 10 μm.

cells and in cells with MT labeled via SiR-BCNK-tubulin at position G45 (Figure 3C). Mild accumulation of MT acetylation was observed at the center of cells labeled at position A278. Systematic quantification of acetylated tubulin signal intensity showed an approximately twofold increase in total MT acetylation in cells labeled with SiR-BCNK-tubulin on positions G45 or A278 (Figure 3C). Notably, an ~1.5 fold increase in cellular MT acetylation was measured in cells transfected with tubulin-GFP (Supplemental Figure S5). It is therefore possible that the observed increase in MT acetylation results, at least in part, from tubulin overexpression.

To measure MT dynamics, COS7 cells were cotransfected with pBUD-BCNK-RS-tub^{G45} and a plasmid encoding a GFP version of the plus-end MT binding protein EB1 (EB1-GFP), and incubated with SiR-Tet. EB1 nicely decorated the plus end of MTs labeled with SiR-BCNK-tubulin (Figure 3D), indicating that the association of MT binding proteins is not perturbed in MT fibers

Assay	Average SNR	% of cells with labeled MTs	
Initial parameters	1.5	5	
Calibrating SiR-Tet concentrations	1.49	5	SiR-Tet concentration: 1 µM
Calibration of BCN-Lys and SiR-Tet washes	1.58	5	Wash duration: 90 min for BCN-Lys + 90 min for SiR-Tet
Calibration of BCN-Lys incubation time	1.58	10	Incubation time: 48 h
Ascorbic acid	1.6	25	Addition of 100 µM ascorbic acid to growth media
Final calibrations	1.75	33	Plasmid optimization

TABLE 1: Calibration of assay conditions.

carrying SiR-BCNK-tubulin. MT growth could be readily detected in cells with SiR-BCNK-tubulin labeled MTs through live cell recording of EB1 dynamics (Figure 3E). Quantitative measurements of EB1 dynamics in these cells showed an average net growth speed of 0.2 ± 0.02 µm/s. This value is within the range of previous measurements performed in tissue culture cells (0.12–0.38 µm/s; Yvon and Wadsworth, 1997; Salaycik *et al.*, 2005; Rosa *et al.*, 2006). A similar growth rate was measured in COS7 cells cotransfected with mCherry-tubulin and EB1-GFP (0.22 ± 0.02 µm/s; Figure 3E). Track length appeared to be somewhat smaller (by 25%) compared to mCherry-tubulin labeled MTs, presumably due to the slight increase in MT acetylation (~2 fold relative to ~1.5 fold; Figure 3C and Supplemental Figure S5). That said, track duration and MT growth angle were similar in cells with MT labeled via SiR-BCNK-tubulin or mCherry-tubulin. Taken together, these results indicate that SFL-TAG is suitable for studying MTs in live mammalian cells.

Encouraged by the validation assays reported above, we set out to record MT dynamics with SiR-BCNK-tubulin. Using the optimized protocol, MTs were video recorded over time for several minutes at ~1 s intervals (Figure 4A and Supplemental Video S1). Additionally, the entire process of mitosis was successfully recorded in HEK293T cells using SiR-BCNK-tubulin and H2B-GFP (Figure 4B and Supplemental Video S2). It therefore appears that SFL-TAG can be used for recording MT dynamics in living cells. Notably, the minimal

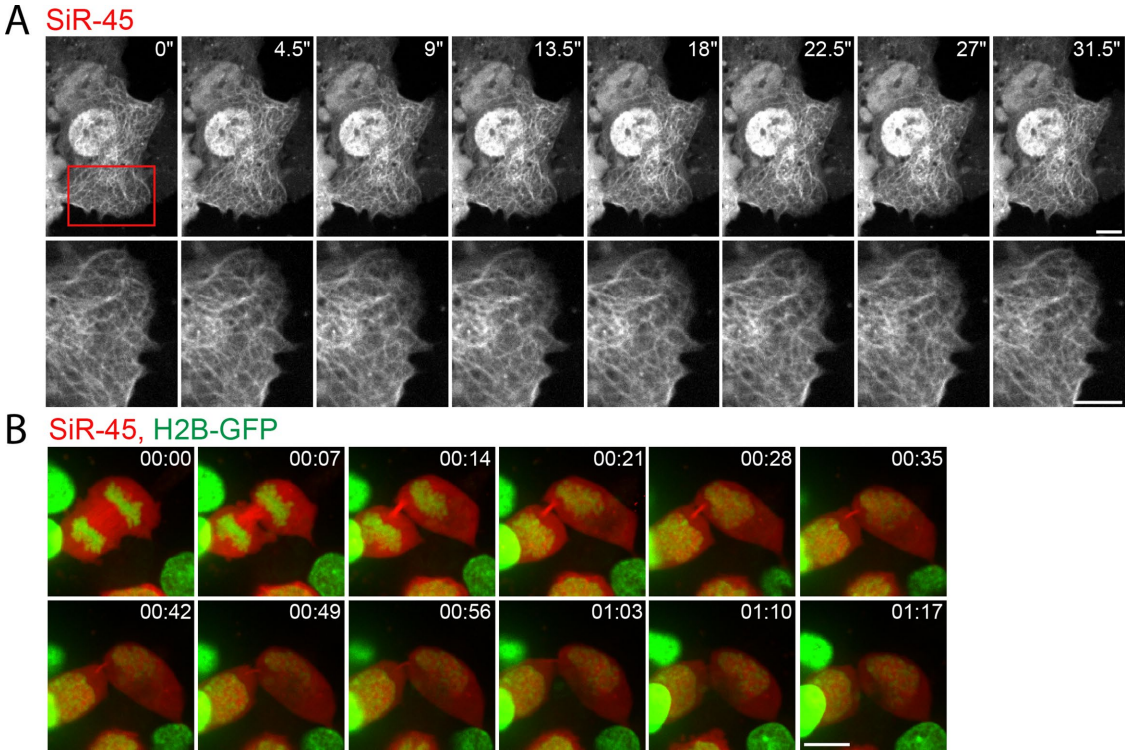

FIGURE 4: Live cell imaging of MTs labeled with SiR-BCNK-tubulin. COS7 cells (A) or HEK293T cells (B) were either single-transfected with pBUD-BCNK-RS-tub^{45TAG} alone (A) or together with H2B-GFP (B), incubated for 48 h in the presence of BCN-Lys, and labeled with SiR-Tet (1 h). (A) Live cell recordings of single Z sections were collected at 1.1 s intervals. Shown are images from every fifth frame of a representative movie series (images correspond to Supplemental Video S1). The bottom panel shows zoomed-in images of a subset of the cell (corresponds to rectangle in upper panel; rotated 90 deg). $n = 7$; scale bar, 10 µm. (B) 3D volumes of dividing HEK293T cells were recorded live at 7 min intervals. Shown are maximum intensity projections of subsequent frames from a representative cell (images correspond to Supplemental Video S2). Notably, spindle microtubules were clearly decorated with SiR-BCNK-tubulin. $n = 9$; scale bar, 10 µm.

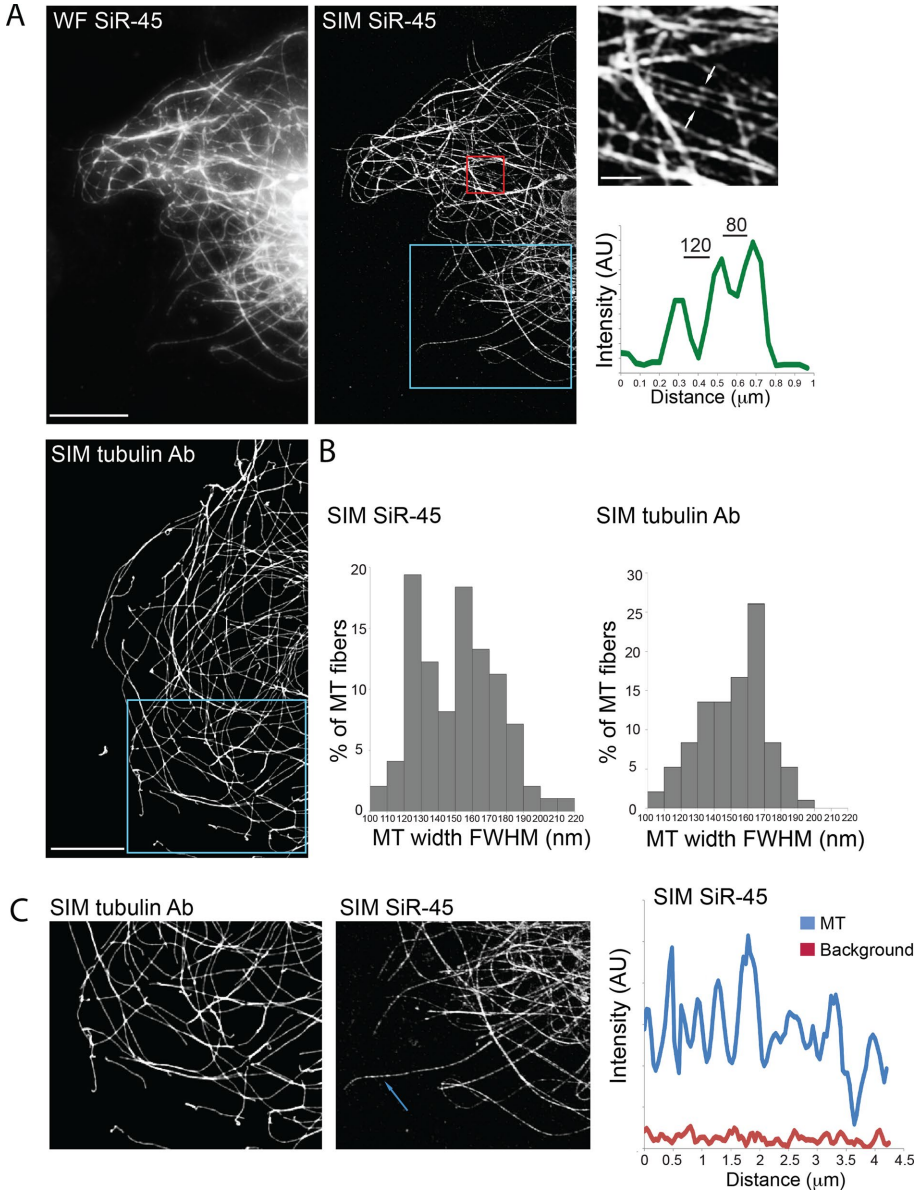

FIGURE 5: SIM imaging of MTs labeled with SiR-BCNK-tubulin. (A–C) COS7 cells were either transfected with pBUD-BCNK-RS-tub^{45TAG} incubated for 48 h in the presence BCN-Lys, and labeled with SiR-Tet (1 h) or stained for endogenous tubulin using α-tubulin primary antibodies and Alexa 647 secondary antibodies. Cells were then fixed, permeabilized, and subjected to 3D SIM imaging as described in *Materials and Methods*. (A) Left to right: a subset of a representative cell in wide field and in SIM (entire cell is shown in Supplemental Figure S6A) and a zoomed-in image of a small region in the SIM image (corresponds to red rectangle) showing three adjacent MT fibers that are resolved in SIM. Intensity profile of a line drawn between the arrows is plotted below the image. Shown are maximum projection images. Bottom panel: a subset of a representative naïve cell stained with α-tubulin antibodies and imaged in SIM (entire cell is shown in Supplemental Figure S6A). Scale bar, 10 μm, zoomed-in image, 1 μm. (B) FWHM of individual MT thickness was measured in different cells. Measurements for each condition were obtained from 100 MT fibers taken from three different cells. (C) Zoomed-in images taken from SIM images (corresponds to cyan rectangles in SIM images) highlighting the inhomogeneity in MT labeling observed in SiR-BCNK-tubulin labeled MTs. Labeling density was measured by drawing a line intensity profile along individual MT fibers and measuring the percent of "non–α-tubulin labeled" regions as described in the main text. Plot on right: line intensity profile along an individual microtubule fiber (see arrow in image) shows the periodicity in labeling observed through SIM in SiR-BCNK-tubulin labeled MTs. Notably, all intensity values measured along the fiber were higher than background levels (compare graphs in plot), indicating that regions defined as "nonlabeled" still contain SiR-BCNK-tubulin labeling.

size of the fluorescent tag is expected to provide a more realistic view on the dynamics of MTs in live cells.

One of the advantages of SFL-TAG is its applicability to SR microscopy. The use of a better fluorophore together with its reduced size hold great potential for increasing both spatial and temporal resolution in these approaches. To examine the applicability of SFL-TAG labeling to SIM, COS7 cells were subjected to MT labeling using SFL-TAG, fixed and imaged by SIM (Figure 5A and Supplemental Figure S6). Almost no photobleaching was observed between the five phases and three rotations acquired to generate the final three-dimensional (3D) high-resolution image, highlighting the superb photophysical properties of the dye. Remarkably, a distance as small as 80 nm (2 pixels) was measured between adjacent fibers (Figure 5A, right). To estimate resolution in a more robust manner, we measured the width of individual MTs and compared it to the MT width obtained in SIM images of MT labeled via antibody staining (Figure 5B). In cells with MTs labeled using SFL-TAG, a characteristic full-width at half-maximum (FWHM) of 120 nm was measured in some cells and of 150 nm in others (see peaks in graph). Using an optimized protocol for MT immunostaining (see *Materials and Methods*) with Alexa 647 secondary antibodies, a characteristic FWHM of 160 nm was obtained (Figure 5B). Considering that the theoretical resolution for a wavelength of 640 nm is ~160 nm, these measurements indicate an increased resolution in SIM combined with SFL-TAG. We attribute this increase in resolution to the smaller size of the tag (a Fl-dye directly attached to the protein compared with primary and secondary antibodies). So far, we have been unable to obtain subdiffraction resolution in live SIM recordings of SiR-BCNK-tubulin labeled MTs. We estimate that this is because background levels are still too high for the SIM processing algorithm. Yet the resolution increase obtained in SIM images of fixed cells highlights the potential of SFL-TAG labeling in SR microcopy applications.

Careful examination of SiR-BCNK-tubulin labeled MTs revealed that the continuous labeling observed for MTs in spinning disk images (Figure 4) appeared nonhomogeneous in SIM (Figure 5C). This difference most probably stems from the increased spatial resolution, which allows differentiating high-density labeled regions from low-density labeled regions. This inhomogeneity in signal intensity was much less prominent in immunostained MTs (compare left and middle panels in Figure 5C), suggesting that the

inhomogeneity reflects a reduced labeling density in SiR-BCNK-tubulin labeled MTs. To estimate the difference in labeling densities we have considered the low-density labeled regions as "nonlabeled" and measured the percentage of fluorescently labeled regions along individual fibers in SIM images of MTs stained with tubulin antibodies or labeled with SiR-BCNK-tubulin. Pixels along the fiber that had intensity values lower than 30% of the maximum intensity value measured in a specific cell were regarded as "nonlabeled" in the calculations. Under this threshold criterion we calculated a 99.7% labeling coverage in immunostained MTs (measured for 180 µm MT length in three cells). The average labeling density for a total of 185 µm MT length, measured in three cells labeled with SiR-BCNK-tubulin, was 81%. This indicates that labeling density using SiR-BCNK-tubulin is ~20% lower than with antibody staining. Notably, intensity values measured in the "nonlabeled" regions were on average threefold higher than background intensity levels measured in cytosolic regions of the cell that were excluded of MTs. This suggests that regions considered as "nonlabeled" were also labeled by SiR, albeit at a lower proportion (i.e., a smaller subset of α-tubulin is labeled within the 40 µm pixel size). Although labeling efficiency can potentially be further improved, this value indicates that SFL-TAG produces a relatively high labeling density and suggests that it can be used in SR imaging as well as in other advanced imaging applications.

In this work we have optimized conditions for robust site-specific labeling of MTs with Fl-dyes in live cells. Our validation experiments, proof-of-concept dynamics recording and SIM imaging, lay the foundations for using SFL-TAG for studying MT dynamics under more realistic conditions and with improved spatiotemporal resolution. Advanced assays, such as fluorescent speckle microscopy (FSM; Danuser and Waterman-Storer, 2003; Gierke *et al.*, 2010; Kamath *et al.*, 2010), can now be employed noninvasively to measure MT dynamics in live cells. Competition assays using tetrazine-NH_2 (Supplemental Figure S2D) can be used to obtain the low labeling density required in some of these techniques. Importantly, our ability to label MTs, one of the most essential cellular components, validates the feasibility of the approach for labeling a variety of proteins and macromolecular complexes in cells.

The aim of this work was to evaluate the feasibility of using SFL-TAG labeling in live cell imaging applications. While going through the process of optimizing reaction conditions, we have noticed the value of the approach but also recognized its limitations. We learned that 1) finding a suitable site for NCAA incorporation is not a limiting factor of the approach but that incorporation efficiency does not guarantee efficient labeling. 2) Consistent with previous publications (Greiss and Chin, 2011; Bianco *et al.*, 2012; Elsasser *et al.*, 2016; Ernst *et al.*, 2016) manipulating cells to incorporate a NCAA into proteins in response to an in-frame amber stop does not lead to major effects on cell viability. 3) The cellular levels of truncated proteins vary between different incorporation sites. Therefore the level of truncated protein should be quantified for each position and care should be taken to minimize the level of these artificial polypeptides and evaluate their effect on cell viability and function. 4) Background levels tend to be higher than in other labeling approaches. This can potentially result from excess tRNA that is charged with the NCAA, which can bind SiR-Tet via the bioorthogonal reaction or from off-target labeling, including suppression of endogenous amber stop codons. So far, we have been unable to achieve the low background levels required for performing live-SIM imaging or for measuring MT growth and retraction rates from individual fibers. 5) The observed nuclear staining currently limits the approach to proteins that are outside the nucleus. 6) Resolution in SR applications is increased when combined with SFL-TAG. 7) Labeling density in SFL-TAG is sufficient to allow SR imaging.

While applying SFL-TAG using our optimized protocol is suitable for some applications, further optimization work is needed in order to make SFL-TAG a common approach for imaging cellular proteins at native conditions. In that respect, it was recently shown that adding a nuclear export signal (NES) to the orthogonal synthetase dramatically reduces nuclear staining in SFL-TAG (Nikic *et al.*, 2016). When needed, this approach can be combined with our optimized assay. Additionally, since the bioorthogonal reaction used in SFL-TAG is fluorogenic by nature, we estimate that the SNR can be further improved. Improving the SNR by exploring the array of available Fl-dyes as well as testing different tetrazine derivatives will undoubtedly expand the outreach of the approach and will ultimately allow measuring protein dynamics at superb spatiotemporal resolution. Finally, although no global cellular phenotypes resulting from NCAA incorporation have been reported so far, this aspect should be investigated more thoroughly, and tools should be developed to minimize any possible cellular effects resulting from the methodology.

MATERIALS AND METHODS

Cell culture

HEK293T, U2OS, HeLa, and COS7 cells were grown in DMEM supplemented with 10% fetal bovine serum (FBS), 2 mM glutamine, 10,000 U/ml penicillin, and 10 mg/ml streptomycin. MDCK cells were grown in MEM supplemented with 5% FBS, 2 mM glutamine, 10,000 U/ml penicillin, and 10 mg/ml streptomycin.

Genetic code expansion and bioorthogonal chemistry in mammalian cells

Twenty-four hours before transfection, cells were plated as follows: Western blot analysis, 30% confluency, 12-well plate (NUNC, Rochester, NY); live imaging, 20% confluency, four-well chamber slide (Ibidi, Martinsried, Germany); immunostaining, 20% confluency, #1.0 coverslips (Menzel, Braunschweig, Germany); SIM, 20% confluency on µ-Dish 35 mm (high, glass bottom, 2 ml; Ibidi, Martinsried, Germany). Transfection was carried out using Lipofectamine 2000 (Life Technologies, Carlsbad, CA) according to the manufacturer's guidelines, with the selected plasmids described in Supplemental Figure S1B. Cells were then incubated for 24–48 h in the presence or absence of either Boc-Lys (1 mM; Chemimpex, Wood Dale, IL) or BCN-Lys (0.5 mM; Synaffix, Oss, Netherlands) in growth media supplemented with 100 µM ascorbic acid (Sigma Aldrich, Israel). After NCAA incubation, the cells were washed with fresh medium (3 × quick wash followed by 3 × 30 min wash) at 37°C and then incubated with SiR-Tet for 1 h at room temperature in the dark (1–2 µM; Spirochrome, Stein am Rhein, Switzerland). Cells were then washed again with fresh medium (3 × quick wash and 3 × 30 min wash) at 37°C. A detailed protocol is provided in the Supplemental Information.

Western blot analysis

Cells were lysed using RIPA lysis buffer (150 mM NaCl, 1% NP-40, 0.5% deoxycholate, 0.1% SDS, 50 mM Tris [pH 8.0]) supplemented with complete protease inhibitor (Roche Diagnostics, Mannheim, Germany) for 30 min at 4°C. Total protein concentrations were measured using the BCA Protein Assay Kit (Pierce Biotechnology, Rockford, IL), and equal total protein amounts were loaded in each lane. Membranes were stained with primary rabbit anti-HA antibodies (1:4000; Applied Biological Materials, Richmond, Canada) for 16 h at 4°C and anti rabbit-peroxidase secondary antibodies for 1 h (1:10,000; Jackson ImmunoResearch, West Grove, PA).

Immunostaining

Cells were fixed with 4% paraformaldehyde (PFA), permeabilized with 0.5% Triton X-100 (in phosphate-buffered saline [PBS]) for 10 min, and blocked with 10% FBS (in PBS) for 15 min. All cells were stained with mouse monoclonal anti-α-tubulin antibodies (1:1000, DM1A; Sigma-Aldrich), rabbit polyclonal anti-HA antibodies (1:500; Applied Biological Materials, Richmond, Canada), or monoclonal anti-acetylated tubulin antibodies (1:1000, 6-11B-1; Sigma-Aldrich). Cells were then subjected to a secondary antibody staining using Alexa Fluor 594 or Alexa Fluor 488 anti-mouse or anti-rabbit secondary antibodies (Life Technologies). Finally, cells were mounted with Fluoromount-G (SouthernBiotech, Birmingham, AL).

Live cell imaging and image processing

COS7 or HEK293T cells were plated as indicated above, transfected 24 h later, and labeled 48 h posttransfection as described above. 3D Z-stacks of selected SiR labeled cells were collected at 37°C using a fully incubated confocal spinning-disk microscope (Marianas; Intelligent Imaging, Denver, CO) with a 63 × oil objective (numerical aperture, 1.4) and were recorded on an electron-multiplying charge-coupled device camera (pixel size, 0.079 µm; Evolve; Photometrics, Tucson, AZ). Image processing and analysis were done using SlideBook version 6 (Intelligent Imaging). For better visualization and tracking of EB1, a Laplacian filter was applied to EB1 channel. Then EB1 particles were tracked using a basic tracking protocol. All measurements were extracted directly from SlideBook. Colocalization analysis was done using Volocity 6 (PerkinElmer, Waltham, MA). Background subtraction was applied before colocalization analysis.

SIM imaging

COS7 cells were plated as indicated above, transfected 24 h later, and labeled 48 h posttransfection as described above. Cells were then washed with prewarmed General Tubulin buffer (GT buffer; Cytoskeleton, Denver, CO), permeabilized for 1 min with 0.2% NP40 (IGEPAL-630; Sigma-Aldrich), and fixed for 10 min using 2 mM of ethyleneglycol-bis-succinimidyl-succinate (EGS; bio-world, Dublin, OH). Both NP40 and EGS solutions were diluted in prewarmed GT buffer. Finally, cells were washed once with PBS, once with PBS containing 100 mM glycine, and once more with PBS. For SIM imaging of immunostained MTs, naïve cells were washed and permeabilized as described above and fixed for 15 min in 3% PFA + 0.1% glutaraldehyde diluted in PBS. Cells were then washed with PBS and permeabilized and blocked with 0.2% Triton X-100 with 3% BSA for 30 min. Cells were stained with monoclonal anti–α-tubulin antibodies (DM1A; Sigma-Aldrich) followed Alexa-647 anti-mouse secondary antibodies (Life Technologies). Finally, cells were postfixed with 3% PFA +0.1% glutaraldehyde and mounted with Fluoromount-G.

Z-stacks (0.144 µm) of selected cells were collected in three rotations using an ELYRA PS.1 microscope (Carl Zeiss MicroImaging, Jena, Germany). Images were reconstructed using ZEN software (Carl Zeiss MicroImaging). To avoid possible reconstruction artifacts resulting from the high staining observed in the nucleus, subsets of the cell (outside the nucleus) were cropped from the raw data set and reconstructed separately. Data analysis and measurements were done only on these cropped reconstructed regions. All measurements were performed on reconstructed superresolution images in ZEN.

Flow cytometry

COS7 or HEK293T cells were grown in six-well plates and transfected with the specified plasmids, as described above. Forty-eight hours later, cells were harvested into 15 ml tubes. Then the cells were washed and labeled with SiR-Tet according to the protocol described above with the exception that between steps, cells were centrifuged at 4°C, 200 × *g* for 5 min and resuspended in the appropriate medium. This step was modified in order to avoid washing dead cells away from the sample. Finally, cells were centrifuged and resuspended in cold PBS. When possible, SiR labeled cells were separated from unlabeled cells, and analysis was performed separately for each population. For dead/live analysis, cells were stained with the Propidium Iodide (PI) kit (MBL), according to the manufacturer's protocol. For positive control of PI staining, naïve cells were incubated at 55°C for 20 min. Flow cytometry was performed on a BD Accuri flow cytometer, and data were analyzed using FlowJo software.

ACKNOWLEDGMENTS

The project leading to this article has received funding from the European Research Council under the European Union's Horizon 2020 research and innovation program under grant agreement No. 639313 and from the U.S. Army Research Office (ARO) under grant agreement No. 65422-LS.

REFERENCES

Bianco A, Townsley FM, Greiss S, Lang K, Chin JW (2012). Expanding the genetic code of Drosophila melanogaster. Nat Chem Biol 8, 748–750.

Blackman ML, Royzen M, Fox JM (2008). Tetrazine ligation: fast bioconjugation based on inverse-electron-demand Diels-Alder reactivity. J Am Chem Soc 130, 13518–13519.

Cohen S, Arbely E (2016). Single-plasmid-based system for efficient noncanonical amino acid mutagenesis in cultured mammalian cells. Chembiochem 17, 1008–1011.

Danuser G, Waterman-Storer CM (2003). Quantitative fluorescent speckle microscopy: where it came from and where it is going. J Microsc 211, 191–207.

Davis L, Chin JW (2012). Designer proteins: applications of genetic code expansion in cell biology. Nature reviews. Mol Cell Biol 13, 168–182.

Elsasser SJ, Ernst RJ, Walker OS, Chin JW (2016). Genetic code expansion in stable cell lines enables encoded chromatin modification. Nat Methods 13, 158–164.

Ernst RJ, Krogager TP, Maywood ES, Zanchi R, Beranek V, Elliott TS, Barry NP, Hastings MH, Chin JW (2016). Genetic code expansion in the mouse brain. Nat Chem Biol 12, 776–778.

Gierke S, Kumar P, Wittmann T (2010). Analysis of microtubule polymerization dynamics in live cells. Methods Cell Biol 97, 15–33.

Greiss S, Chin JW (2011). Expanding the genetic code of an animal. J Am Chem Soc 133, 14196–14199.

Henriques R, Griffiths C, Hesper Rego E, Mhlanga MM (2011). PALM and STORM: unlocking live-cell super-resolution. Biopolymers 95, 322–331.

Johnson JA, Lu YY, Van Deventer JA, Tirrell DA (2010). Residue-specific incorporation of non-canonical amino acids into proteins: recent developments and applications. Curr Opin Chem Biol 14, 774–780.

Kamath K, Oroudjev E, Jordan MA (2010). Determination of microtubule dynamic instability in living cells. Methods Cell Biol 97, 1–14.

Kleiner RE, Ti SC, Kapoor TM (2013). Site-specific chemistry on the microtubule polymer. J Am Chem Soc 135, 12520–12523.

Lang K, Chin JW (2014). Cellular incorporation of unnatural amino acids and bioorthogonal labeling of proteins. Chem Rev 114, 4764–4806.

Lang K, Davis L, Torres-Kolbus J, Chou C, Deiters A, Chin JW (2012a). Genetically encoded norbornene directs site-specific cellular protein labelling via a rapid bioorthogonal reaction. Nat Chem 4, 298–304.

Lang K, Davis L, Wallace S, Mahesh M, Cox DJ, Blackman ML, Fox JM, Chin JW (2012b). Genetic Encoding of bicyclononynes and trans-cyclooctenes for site-specific protein labeling in vitro and in live mammalian cells via rapid fluorogenic Diels-Alder reactions. J Am Chem Soc 134, 10317–10320.

Lukinavicius G, Umezawa K, Olivier N, Honigmann A, Yang G, Plass T, Mueller V, Reymond L, Correa IR Jr, Luo ZG, *et al*. (2013). A near-infrared fluorophore for live-cell super-resolution microscopy of cellular proteins. Nat Chem 5, 132–139.

Nikic I, Estrada Girona G, Kang JH, Paci G, Mikhaleva S, Koehler C, Shymanska NV, Ventura Santos C, Spitz D, Lemke EA (2016). Debugging eukaryotic genetic code expansion for site-specific click-PAINT super-resolution microscopy. Angew Chemie 55, 16172–16176.

Nikic I, Lemke EA (2015). Genetic code expansion enabled site-specific dual-color protein labeling: superresolution microscopy and beyond. Curr Opin Chem Biol 28, 164–173.

Peng T, Hang HC (2016). Site-specific bioorthogonal labeling for fluorescence imaging of intracellular proteins in living cells. J Am Chem Soc 138, 14423–14433.

Plass T, Milles S, Koehler C, Szymanski J, Mueller R, Wiessler M, Schultz C, Lemke EA (2012). Amino acids for Diels-Alder reactions in living cells. Angew Chemie 51, 4166–4170.

Pott M, Schmidt MJ, Summerer D (2014). Evolved sequence contexts for highly efficient amber suppression with noncanonical amino acids. ACS Chem Biol 9, 2815–2822.

Reymond L, Lukinavicius G, Umezawa K, Maurel D, Brun MA, Masharina A, Bojkowska K, Mollwitz B, Schena A, Griss R, Johnsson K (2011). Visualizing biochemical activities in living cells through chemistry. Chimia 65, 868–871.

Rosa J, Canovas P, Islam A, Altieri DC, Doxsey SJ (2006). Survivin modulates microtubule dynamics and nucleation throughout the cell cycle. Mol Biol Cell 17, 1483–1493.

Salaycik KJ, Fagerstrom CJ, Murthy K, Tulu US, Wadsworth P (2005). Quantification of microtubule nucleation, growth and dynamics in wound-edge cells. J Cell Sci 118, 4113–4122.

Uttamapinant C, Howe JD, Lang K, Beranek V, Davis L, Mahesh M, Barry NP, Chin JW (2015). Genetic code expansion enables live-cell and super-resolution imaging of site-specifically labeled cellular proteins. J Am Chem Soc 137, 4602–4605.

van de Linde S, Heilemann M, Sauer M (2012). Live-cell super-resolution imaging with synthetic fluorophores. Annu Rev Phys Chem 63, 519–540.

Yanagisawa T, Ishii R, Fukunaga R, Kobayashi T, Sakamoto K, Yokoyama S (2008). Multistep engineering of pyrrolysyl-tRNA synthetase to genetically encode N(epsilon)-(o-azidobenzyloxycarbonyl) lysine for site-specific protein modification. Chem Biol 15, 1187–1197.

Yvon AM, Wadsworth P (1997). Non-centrosomal microtubule formation and measurement of minus end microtubule dynamics in A498 cells. J Cell Sci 110(Pt 19), 2391–2401.